Supplement of Hydrol. Earth Syst. Sci., 26, 2779–2796, 2022
https://doi.org/10.5194/hess-26-2779-2022-supplement

Hydrology and Earth System Sciences
Open Access
EGU

Supplement of

Effects of spatial and temporal variability in surface water inputs on streamflow generation and cessation in the rain–snow transition zone

Leonie Kiewiet et al.

Correspondence to: Leonie Kiewiet (leoniekiewiet@gmail.com)

Supplemental material for Kiewiet et al. "Effects of spatial and temporal variability in surface water inputs on streamflow generation and cessation in the rain-snow transition zone" in HESS

Contents of this file

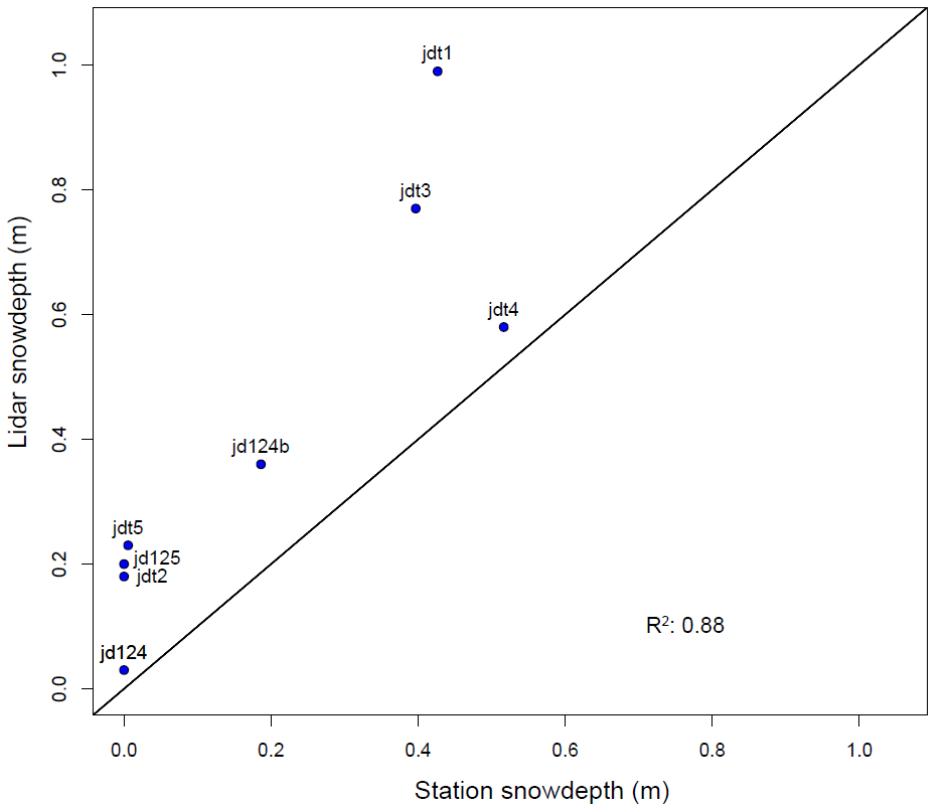

Figure S1: Scatter plot of lidar snow depths and weather station snow depths. See Figure 1 in the main text for locations of each station within the catchment.

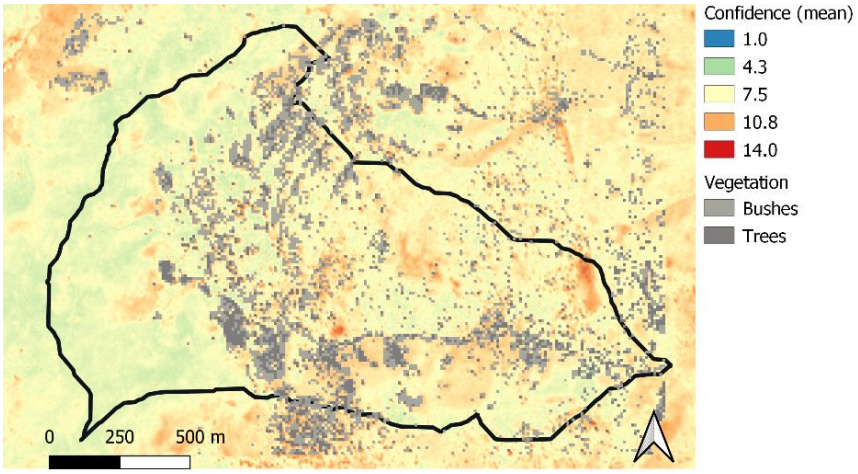

Figure S2: Map of mean confidence levels of snow cover classification using the Maximum Likelihood Classification tool in ArcMap, where blue and green colors indicate higher confidence levels, and orange and red colors lower confidence levels. Vegetated areas are shaded in light grey (bushes) and dark grey (trees).

Table S3: Annual precipitation (P, mm), snowfall fractions (SF, -) and air temperature (T_a, °C), as well as % of the mean of the 2004-2014 record (Godsey et al., 2018). Simulated years are bolded and the year with available lidar is italicized.

Year(s)	P (mm)	% P	SF (-)	% SF	T_a (°C)	% T_a
2004-2014	524	100	0.37	100	8.2	100
2004	470	90	0.49	132	8.4	103
2005	**543**	**104**	**0.23**	**63**	**8.2**	**100**
2006	714	136	0.29	78	8.4	103
2007	402	77	0.31	83	9.3	113
2008	465	89	0.45	123	7.4	91
2009	***549***	***105***	***0.49***	***132***	***8.0***	***98***
2010	**531**	**101**	**0.57**	**155**	**6.6**	**81**
2011	**693**	**132**	**0.41**	**111**	**7.4**	**91**
2012	494	94	0.24	64	8.6	105
2013	456	87	0.26	72	8.6	105
2014	**450**	**86**	**0.30**	**82**	**8.6**	**105**

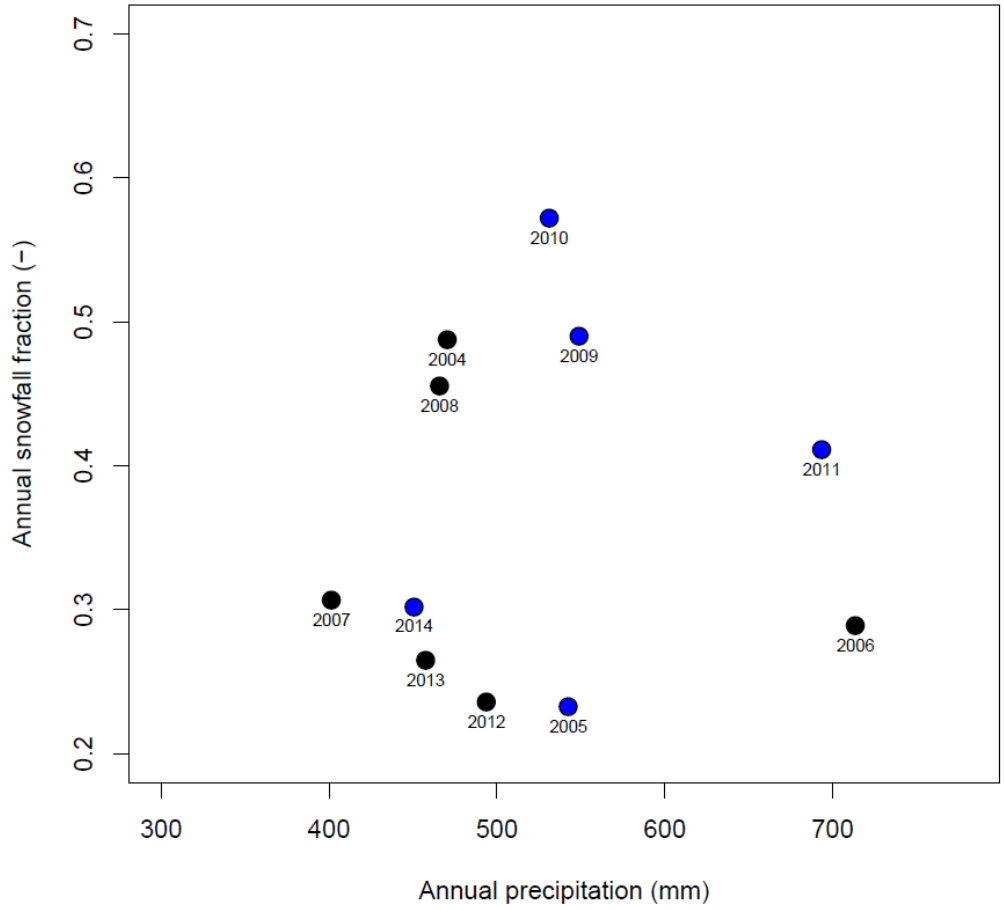

Figure S4: Scatterplot of the annual precipitation and snowfall fraction of precipitation at weather station jd125, which is located close to the catchment outlet. Simulated years are shown in blue, other years are shown in black.

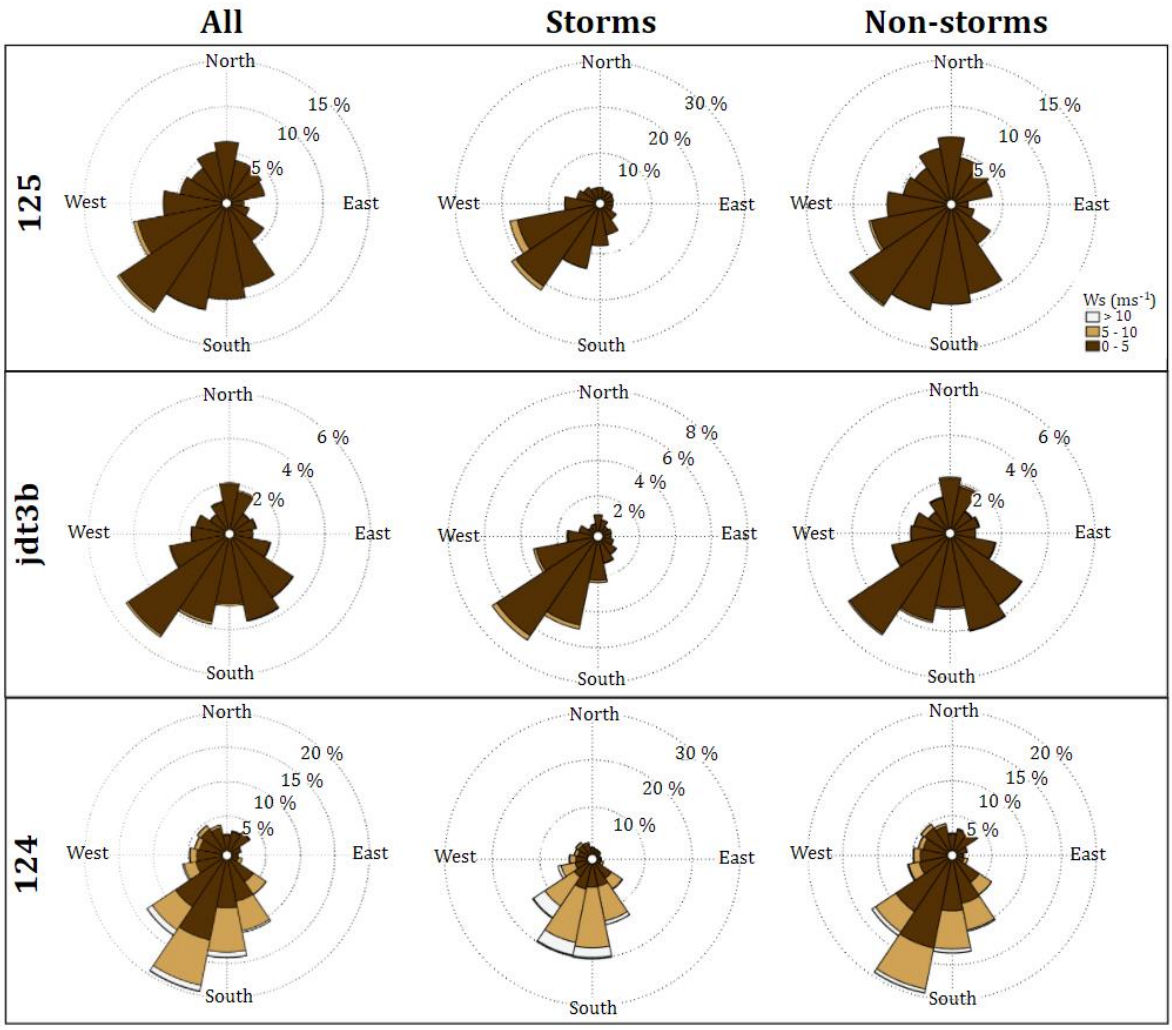

Figure S5: Wind roses for stations jd125 (near the catchment outlet), 124 (near the ridge) and jdt3b (a mid-elevation station on the south-facing slope), compiled with data from 2004-2014 (Godsey et al., 2018). The left column includes all measurements, whereas the center and right columns only include measurements during storms and storm-free periods, respectively. White indicates high wind speeds (> 10 m s^{-1}) whereas orange shows intermediate (5-10 m s^{-1}) and brown shows low (0-5 m s^{-1}) wind speeds. Wind directions during storm events were consistently from the south-southwest.

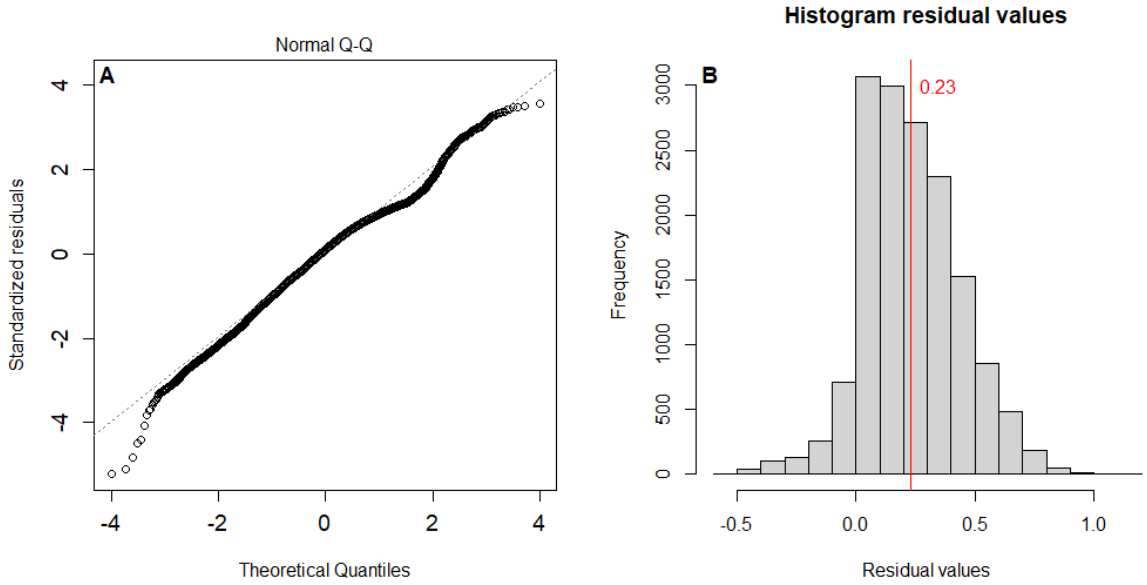

Figure S6: (A) Q-Q plot of the linear model between observed (lidar-derived) and simulated snow depths, and (B) a histogram of the residual values of the observed minus the simulated snow depths in meters, with the mean residual value indicated in red.

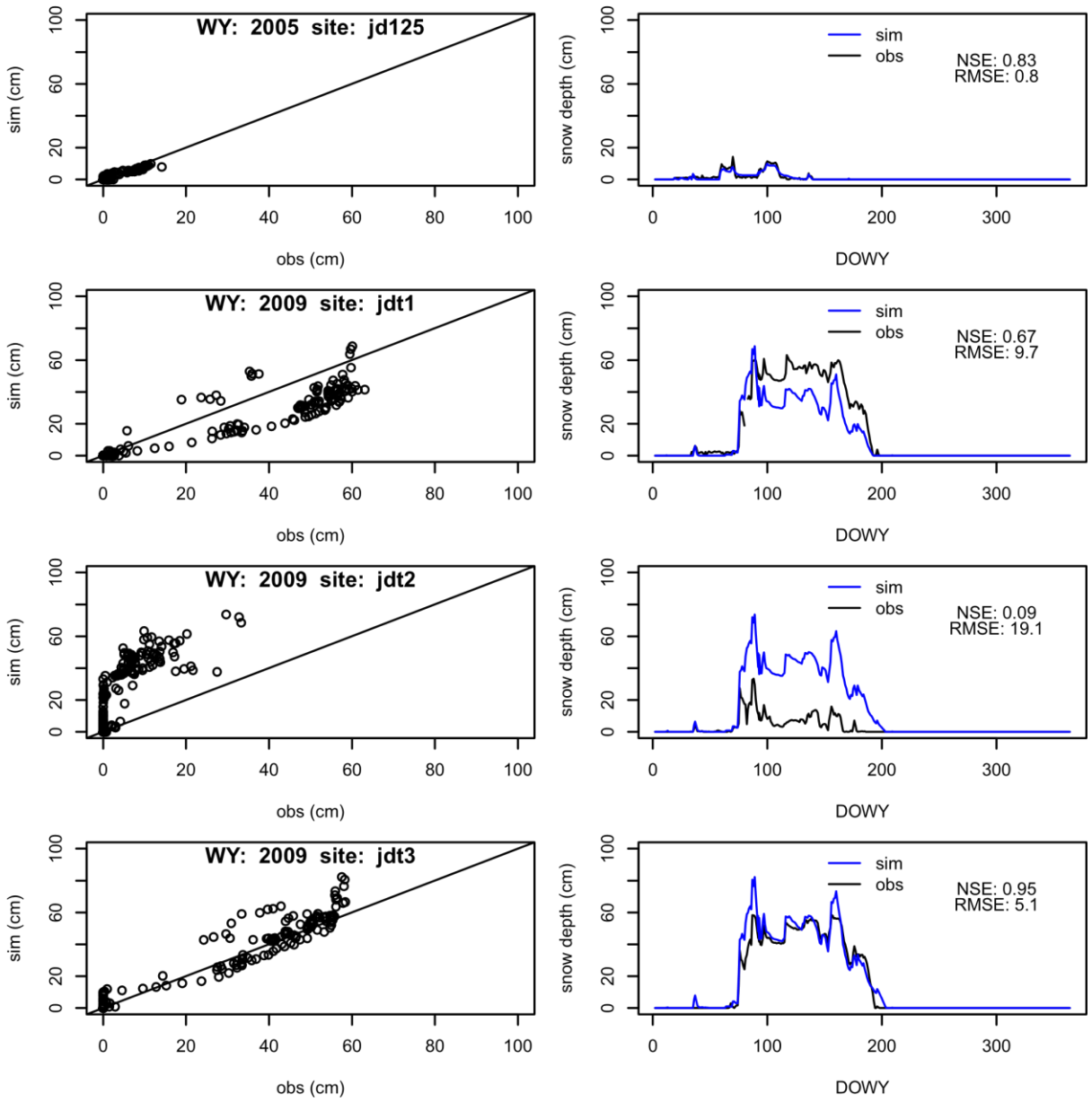

Figure S7a: Scatter plots (left) and time series (right) of observed (obs, black) and simulated (sim, blue) snow depths for 2005 and 2009 for different sites. Water years (WY) and site code for each row are shown in the left column, and Nash-Sutcliffe Efficiency (NSE) and Root Mean Square Error (RMSE) are shown in the right column for each pair of site-year plots.

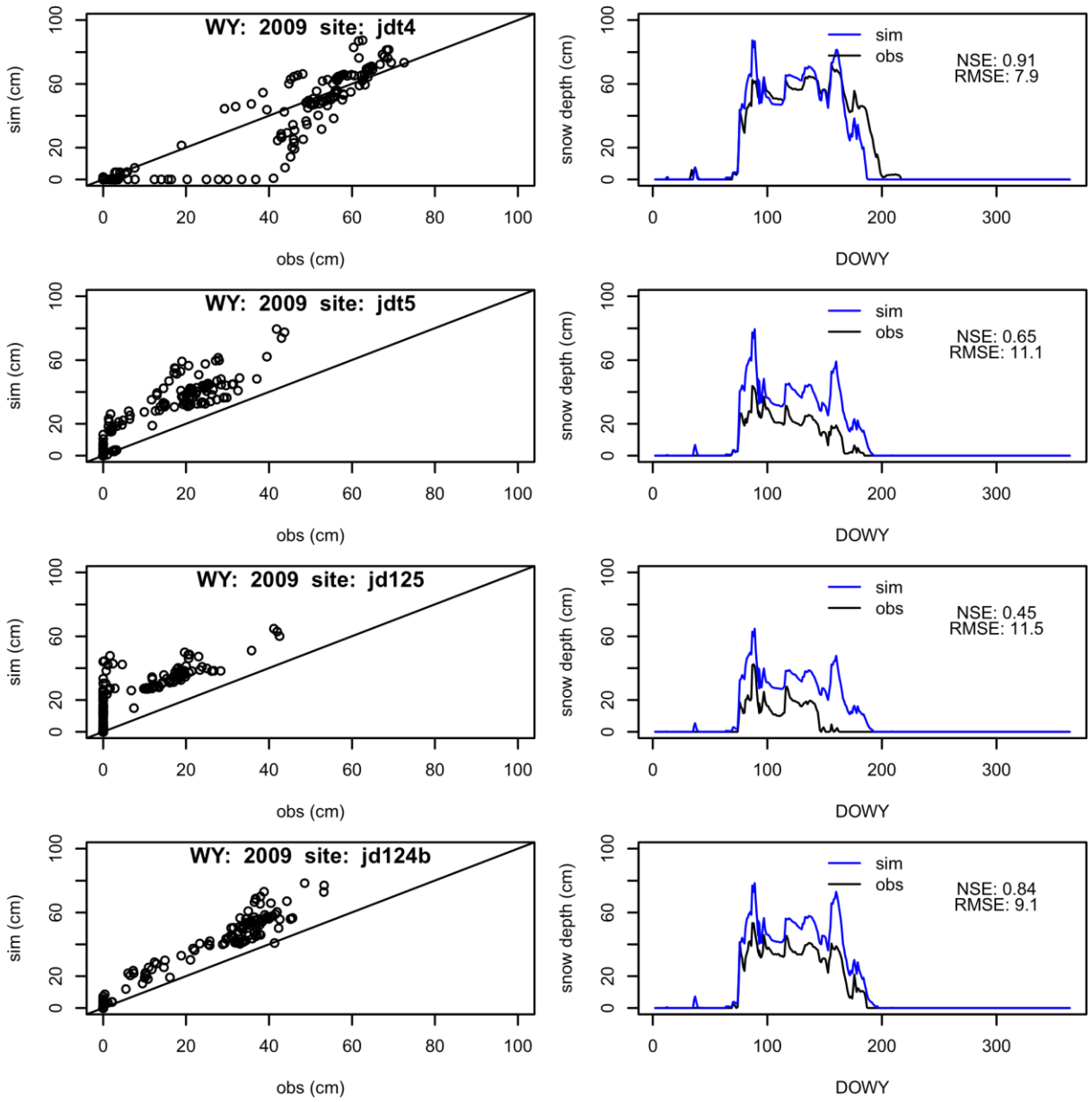

Figure S7b: Scatter plots (left) and time series (right) of observed (obs, black) and simulated (sim, blue) snow depths for 2009 for different sites. Water years (WY) and site code for each row are shown in the left column, and Nash-Sutcliffe Efficiency (NSE) and Root Mean Square Error (RMSE) are shown in the right column for each pair of site-year plots.

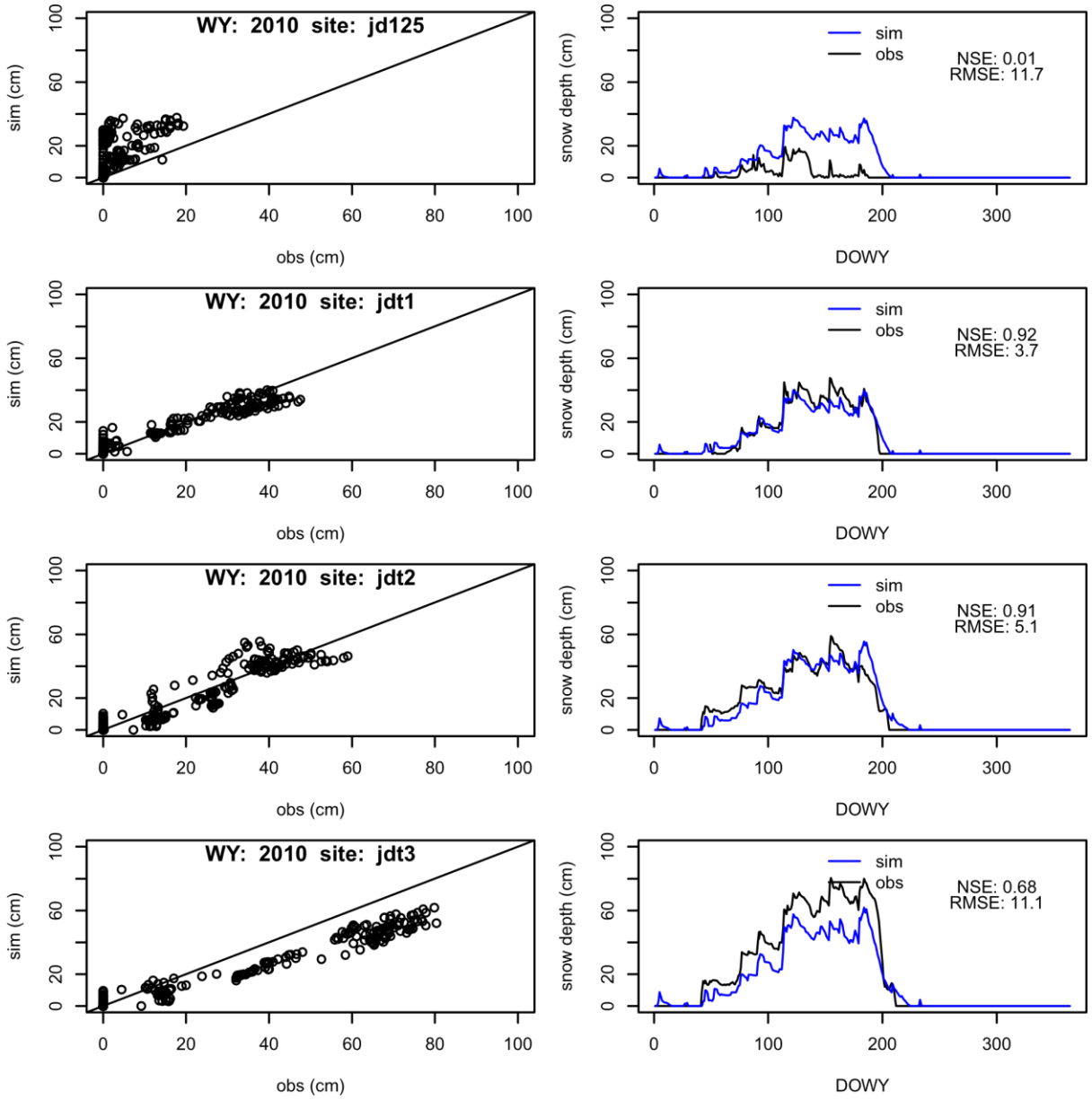

Figure S7c: Scatter plots (left) and time series (right) of observed (obs, black) and simulated (sim, blue) snow depths for 2010 for different sites. Water years (WY) and site code for each row are shown in the left column, and Nash-Sutcliffe Efficiency (NSE) and Root Mean Square Error (RMSE) are shown in the right column for each pair of site-year plots.

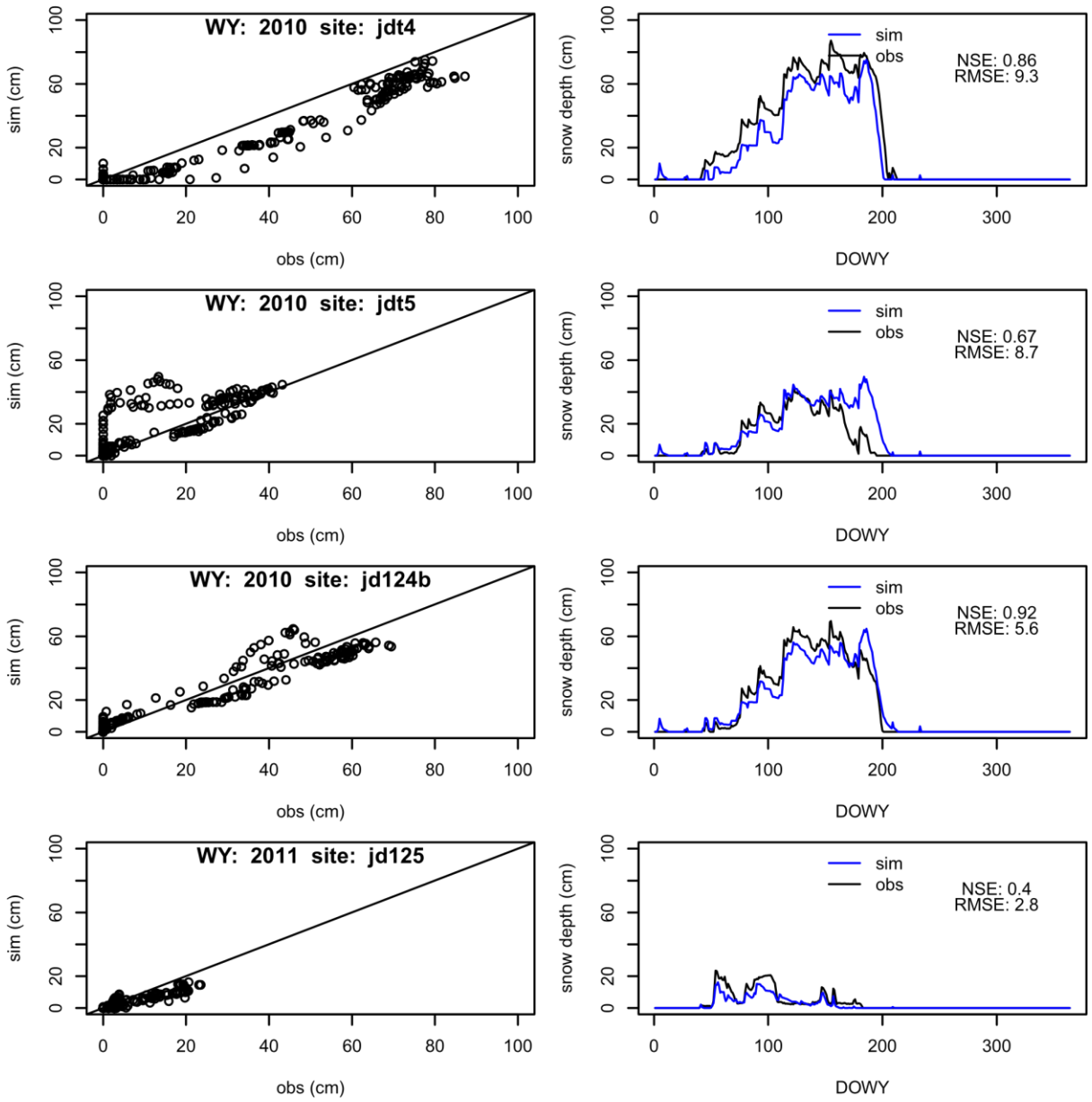

Figure S7d: Scatter plots (left) and time series (right) of observed (obs, black) and simulated (sim, blue) snow depths for 2010 and 2011 for different sites. Water years (WY) and site code for each row are shown in the left column, and Nash-Sutcliffe Efficiency (NSE) and Root Mean Square Error (RMSE) are shown in the right column for each pair of site-year plots.

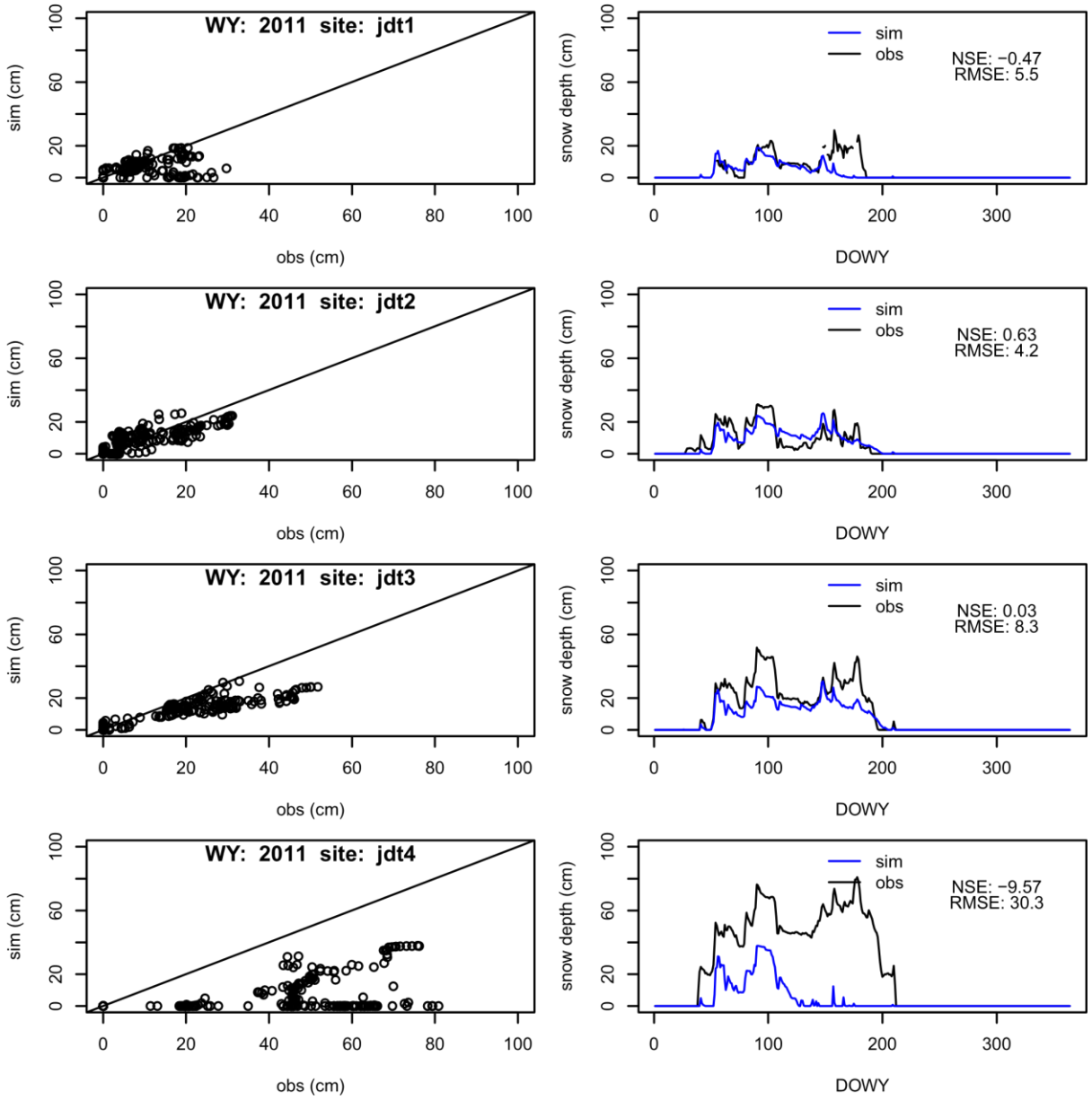

Figure S7e: Scatter plots (left) and time series (right) of observed (obs, black) and simulated (sim, blue) snow depths for 2011 for different sites. Water years (WY) and site code for each row are shown in the left column, and Nash-Sutcliffe Efficiency (NSE) and Root Mean Square Error (RMSE) are shown in the right column for each pair of site-year plots.

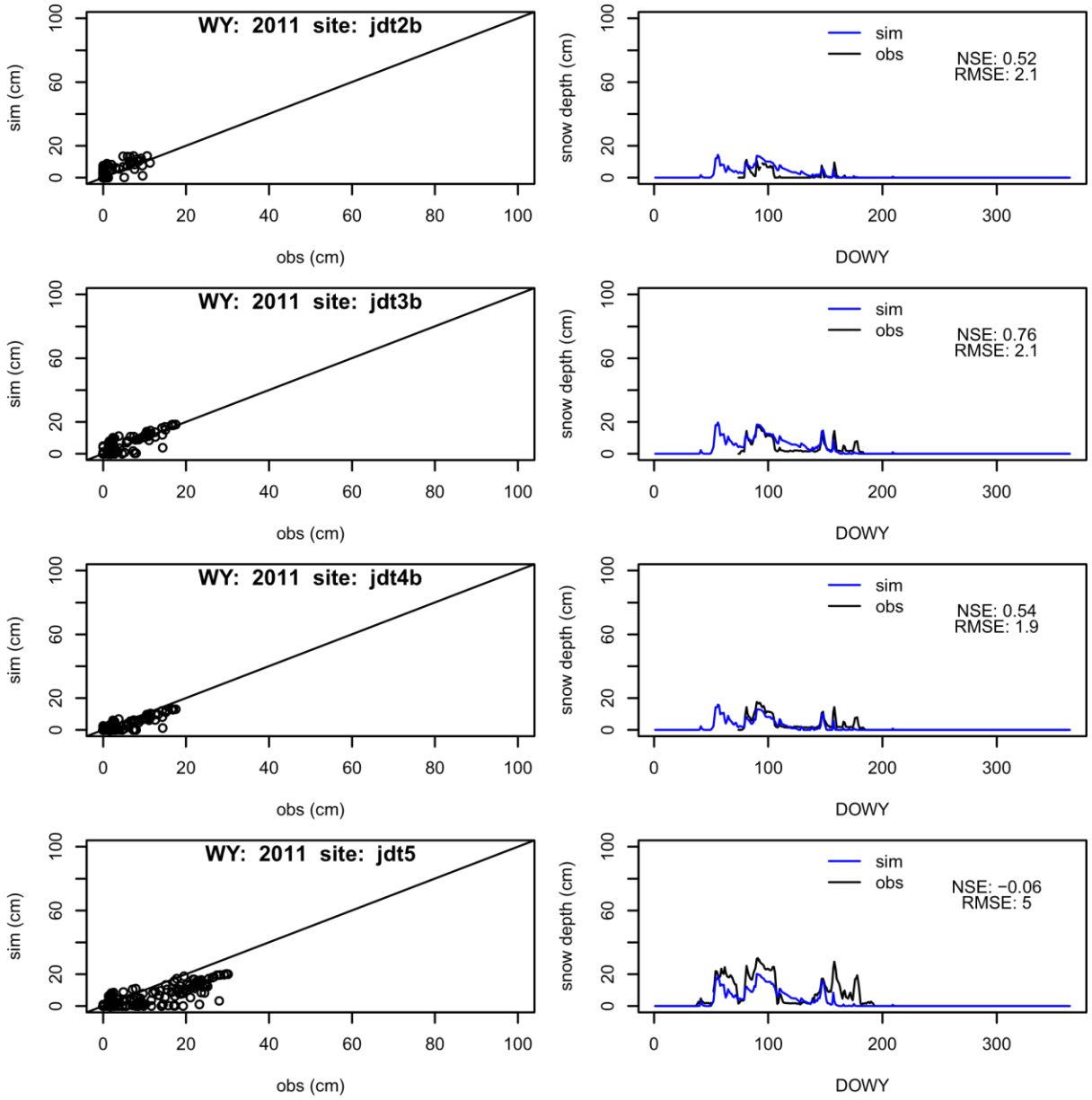

Figure S7f: Scatter plots (left) and time series (right) of observed (obs, black) and simulated (sim, blue) snow depths for 2011 for different sites. Water years (WY) and site code for each row are shown in the left column, and Nash-Sutcliffe Efficiency (NSE) and Root Mean Square Error (RMSE) are shown in the right column for each pair of site-year plots.

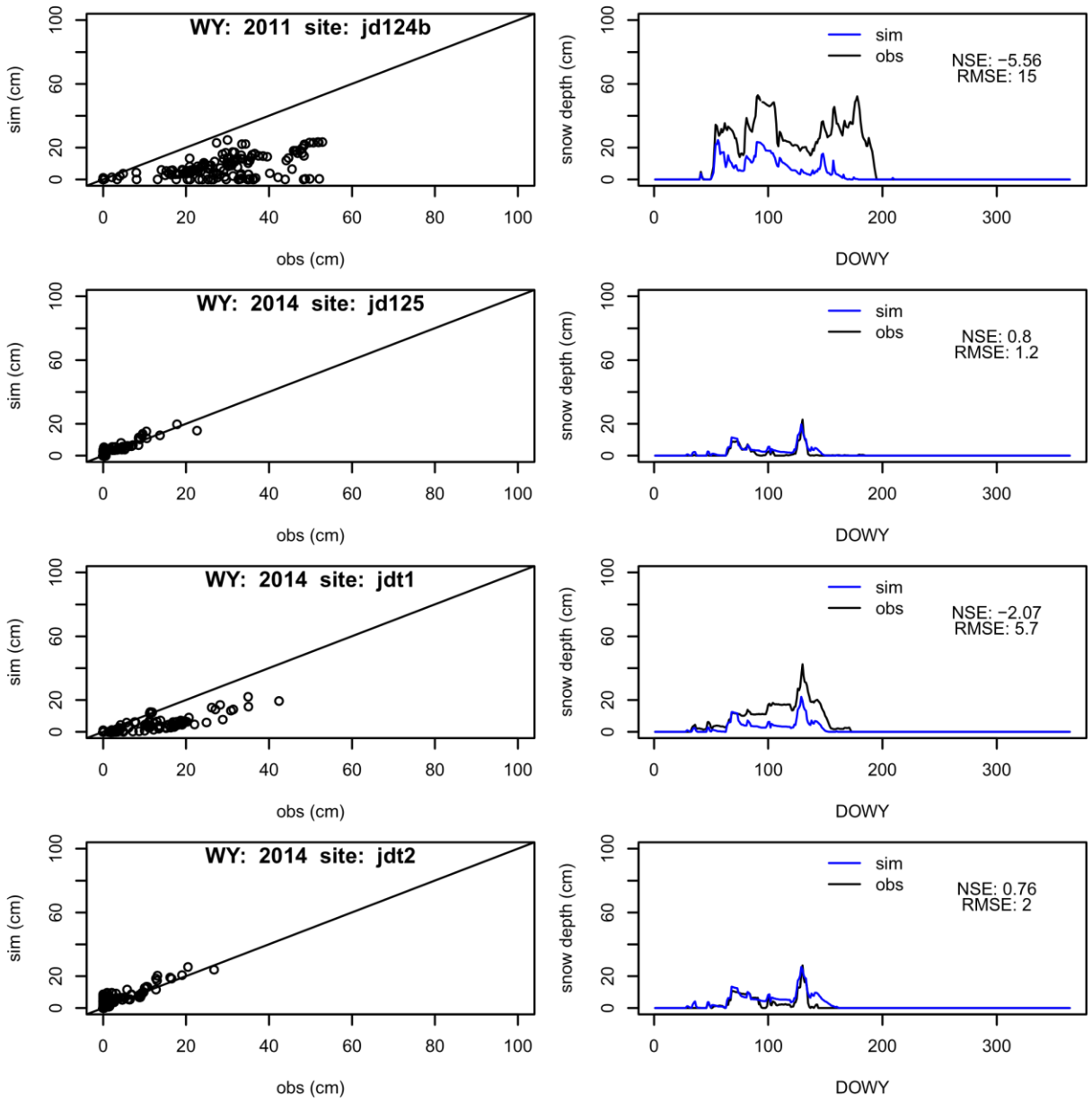

Figure S7g: Scatter plots (left) and time series (right) of observed (obs, black) and simulated (sim, blue) snow depths for 2011 and 2014 for different sites. Water years (WY) and site code for each row are shown in the left column, and Nash-Sutcliffe Efficiency (NSE) and Root Mean Square Error (RMSE) are shown in the right column for each pair of site-year plots.

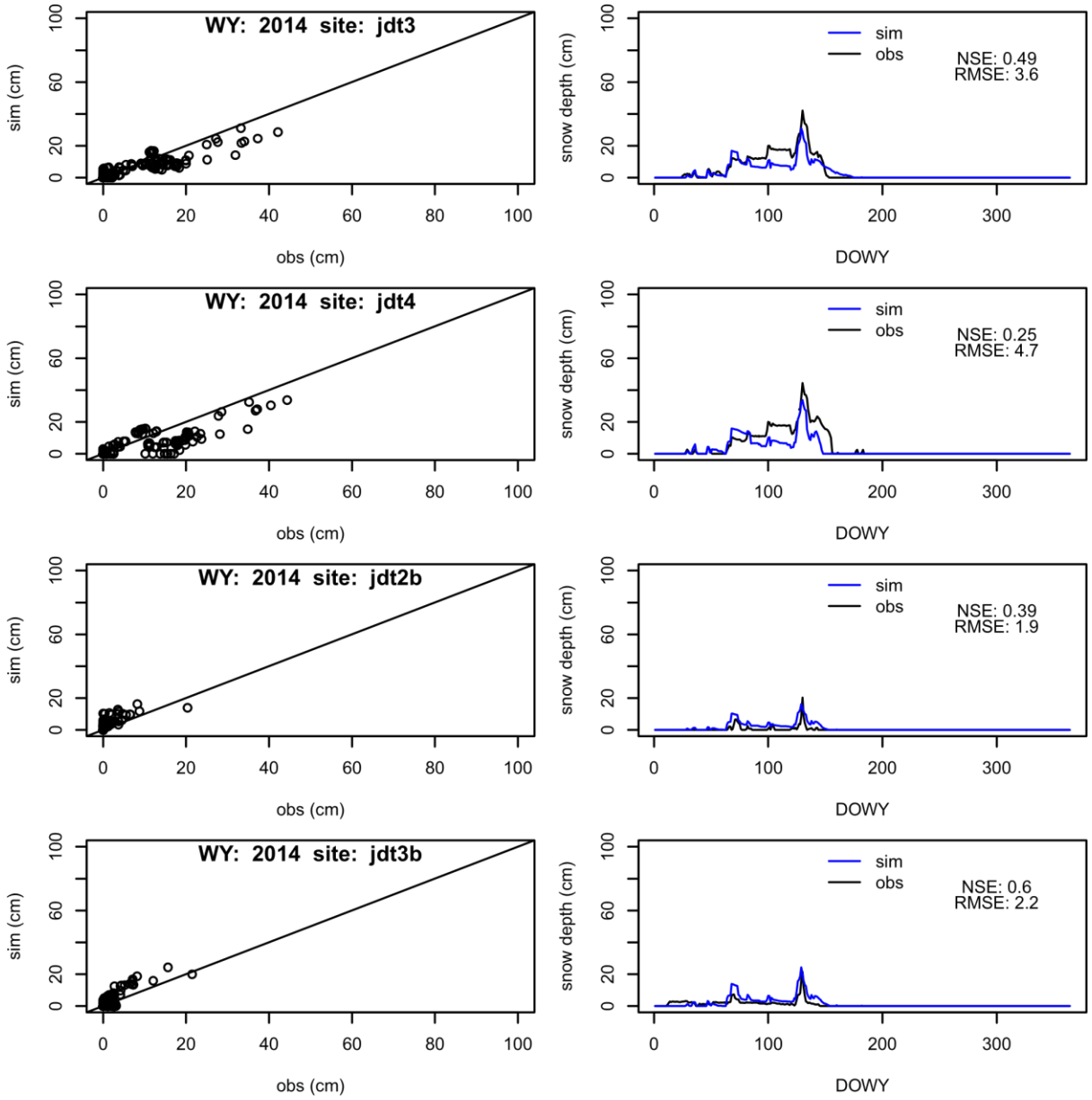

Figure S7h: Scatter plots (left) and time series (right) of observed (obs, black) and simulated (sim, blue) snow depths for 2014 for different sites. Water years (WY) and site code for each row are shown in the left column, and Nash-Sutcliffe Efficiency (NSE) and Root Mean Square Error (RMSE) are shown in the right column for each pair of site-year plots.

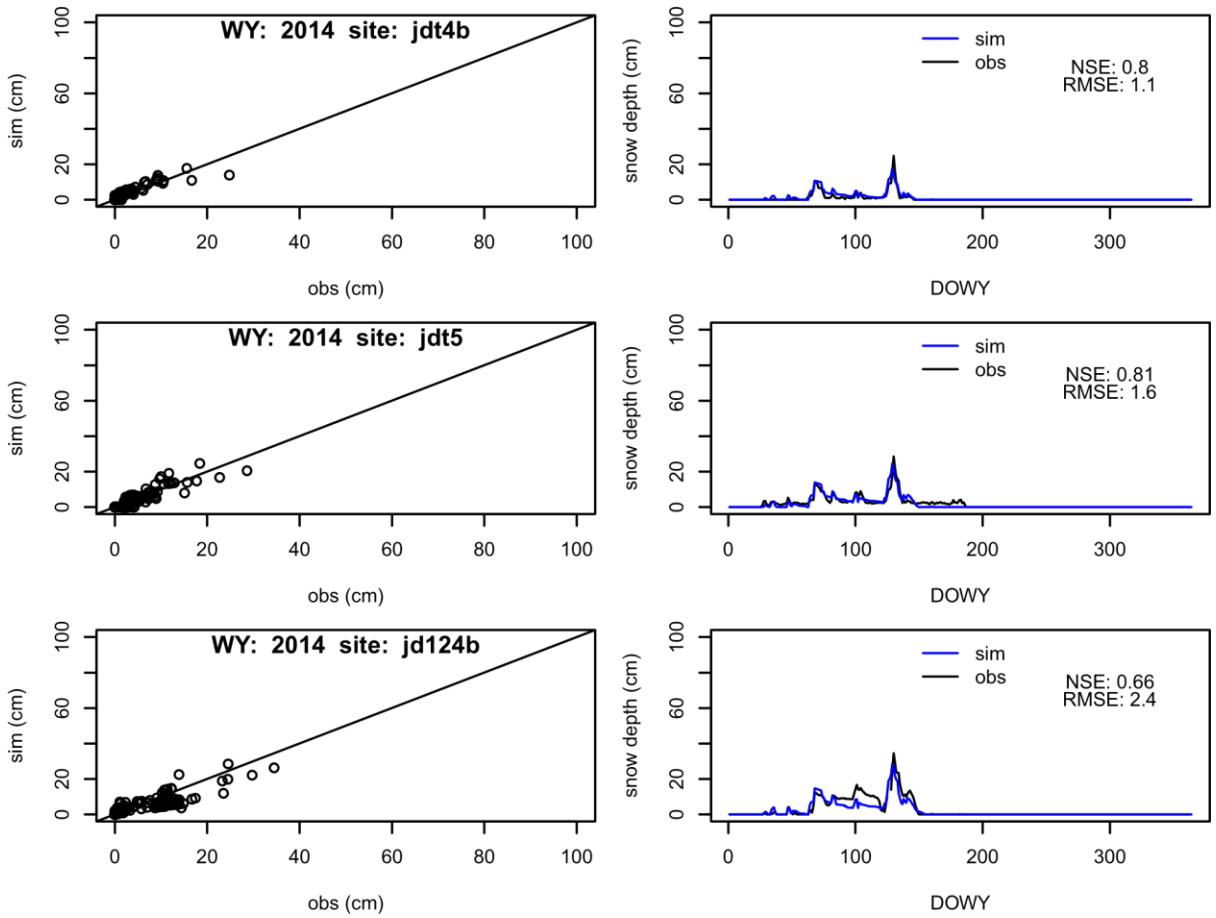

Figure S7i: Scatter plots (left) and time series (right) of observed (obs, black) and simulated (sim, blue) snow depths for 2014 for different sites. Water years (WY) and site code for each row are shown in the left column, and Nash-Sutcliffe Efficiency (NSE) and Root Mean Square Error (RMSE) are shown in the right column for each pair of site-year plots.

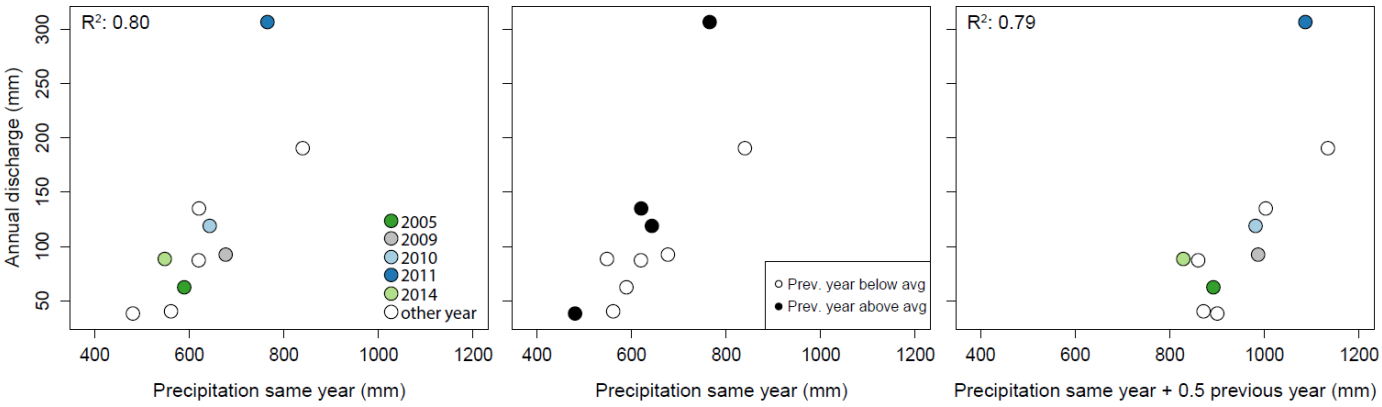

Figure S8: Scatter plots of annual precipitation vs. annual discharge. The left and middle panels show precipitation recorded in the same year as discharge, and the right panel shows precipitation recorded in the same year as discharge + 0.5 times precipitation recorded in the preceding year. In the left- and right-most panels, colored circles indicate years that have been simulated and white circles indicate additional years that have not been simulated. In the center panel, filled symbols indicate years that were preceded by a year with above-average precipitation and open circles are years that were preceded by a year with below-average precipitation.

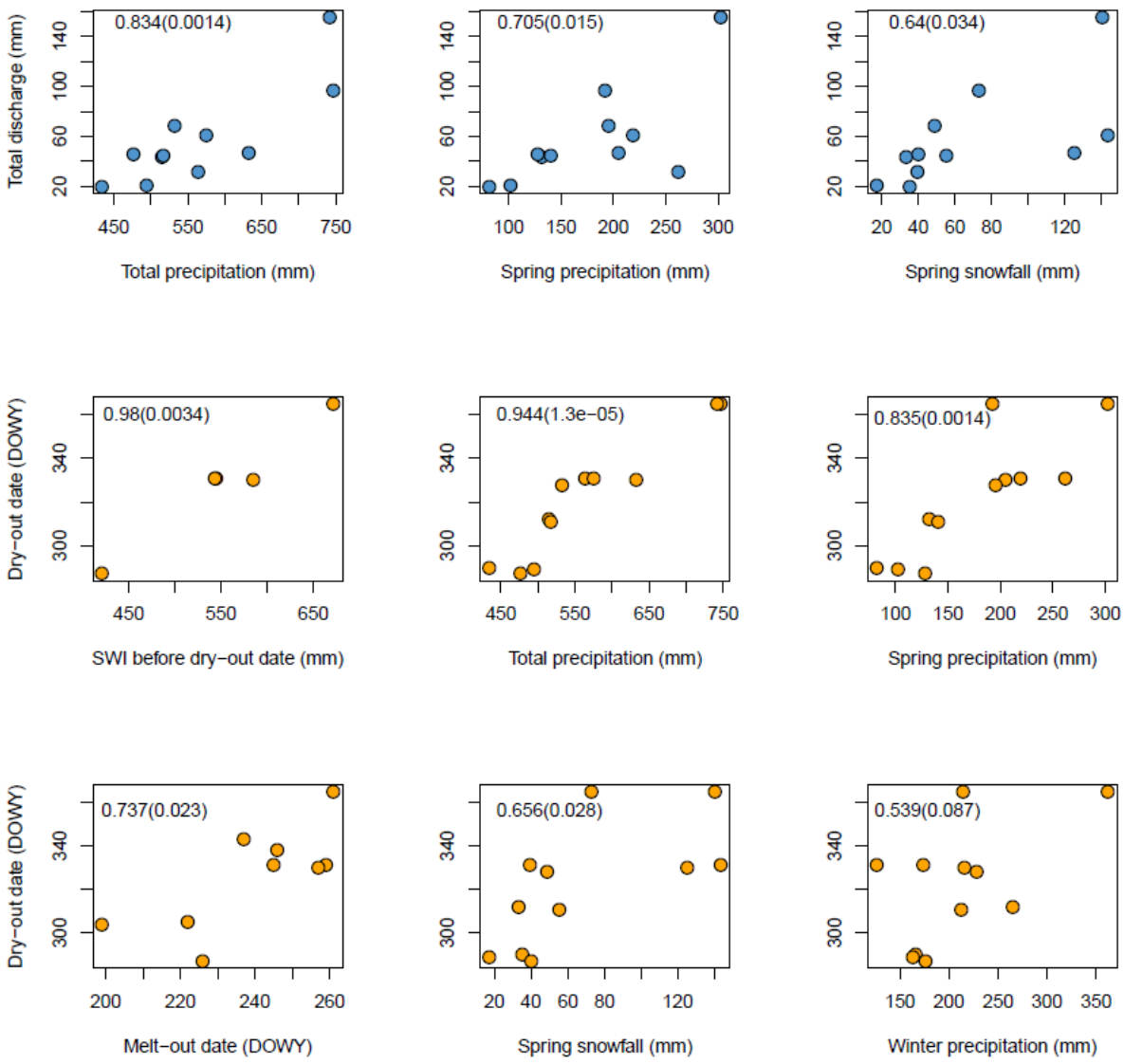

Figure S9: Scatter plots of statistically significant comparisons between precipitation, SWI and snowpack metrics and total discharge (blue circles) and the stream dry-out date (orange circles). Pearson correlation coefficients (r) are given at the top right of each panel, with the corresponding p-value in parentheses.

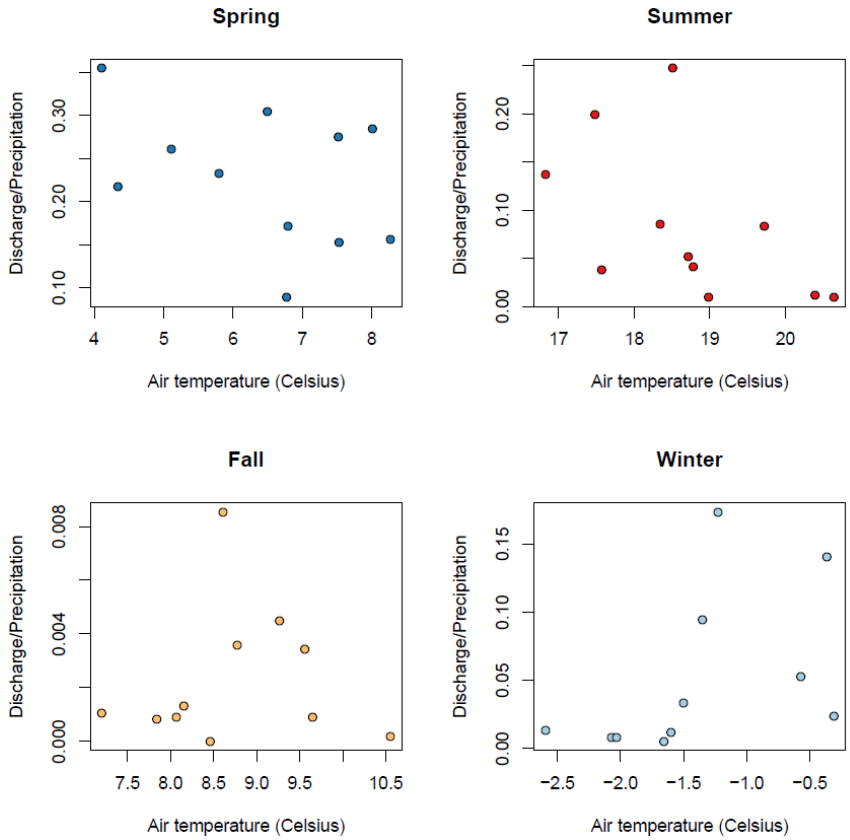

Figure S10: Seasonal air temperatures (°C) versus runoff efficiencies (discharge/precipitation, mm mm^{-1}).

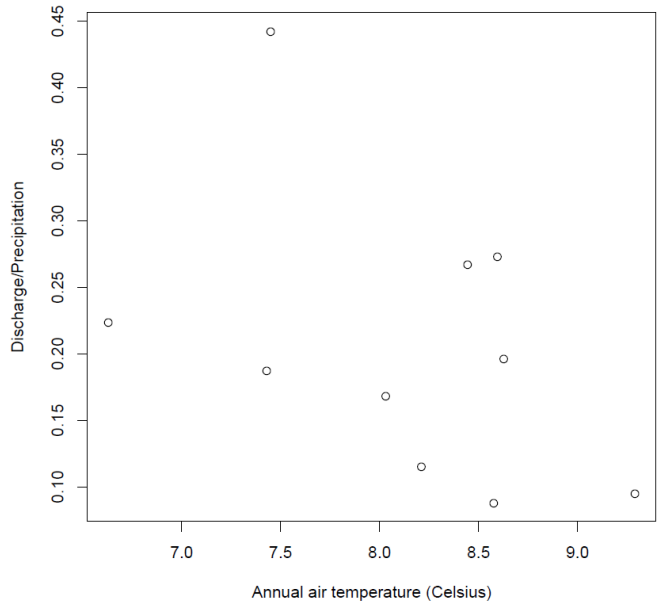

Figure S11: Annual air temperature (°C) versus runoff efficiency (discharge/precipitation, mm mm^{-1}).

Table S12: Average and weighted average of snow densities (Density, simulated) and wind speed (W_s, observed) and direction (W_d, observed) during events with an average snowfall fraction of more than 0.2 for each water year.

WY	Average			Precipitation-weighted average		
	Density (kg m^{-2})	W_s (m s^{-1})	W_d (°)	Density (kg m^{-2})	W_s (m s^{-1})	W_d (°)
2005	124	4.1	187	162	4.8	202
2009	102	5.6	245	102	6.5	252
2010	24	6.6	269	45	8.1	272
2011	117	5.5	232	122	5.7	246
2014	115	6.0	258	126	6.1	266

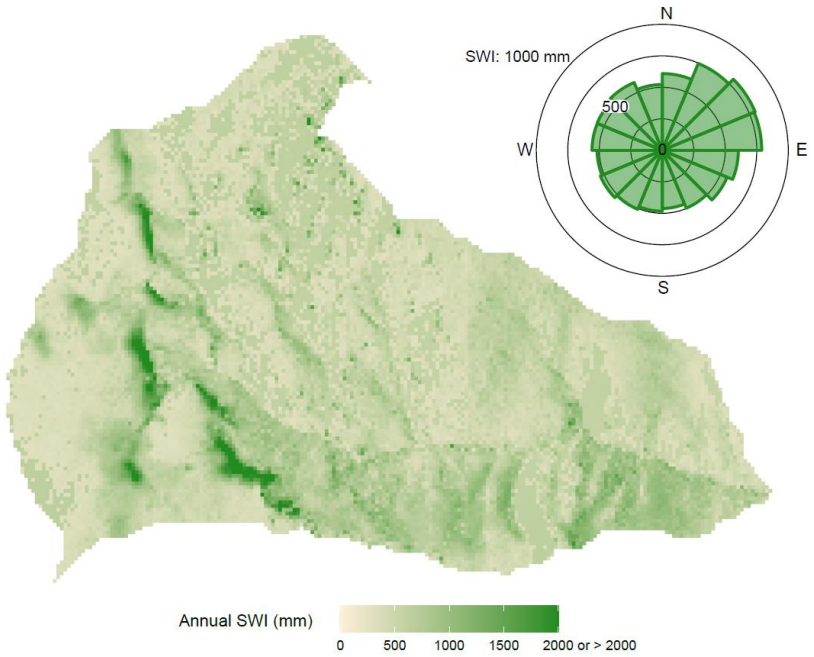

Figure S13: Map showing yearly sum of surface water inputs (SWI, mm) for 2009, with a polar diagram showing the average sum of SWI per 10-m grid cell for each aspect (binned per 22.5°). Higher SWI values are shown in darker colors, lower SWI values in lighter colors, and SWI values are capped at 2000 mm to enhance the contrast.

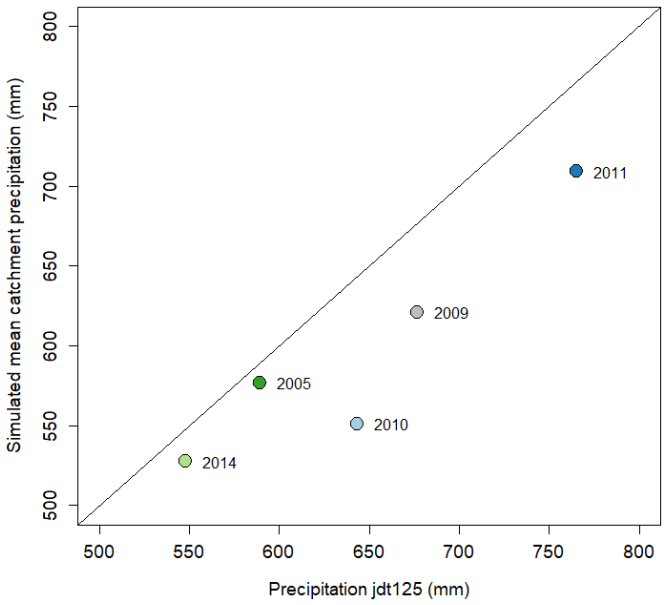

S14: Simulated mean catchment precipitation versus precipitation at jdt125 (the low elevation precipitation gauge) for the years that were modeled.